Mathematical Biosciences 357 (2023) 108969

Contents lists available at ScienceDirect

Mathematical Biosciences

journal homepage: www.elsevier.com/locate/mbs

Original Research Article

Metabolic blood flow regulation in a hybrid model of the human retinal microcirculation

Amanda Albright [a], Brendan C. Fry [b], Alice Verticchio [c], Brent Siesky [c], Alon Harris [c,1], Julia Arciero [a,*,1]

[a] Department of Mathematical Sciences, Indiana University-Purdue University Indianapolis, 402 N. Blackford St, LD 270, Indianapolis, IN 46202, USA
[b] Department of Mathematics and Statistics, Metropolitan State University of Denver, P.O. Box 173362, Campus Box 38, Denver, CO 80217, USA
[c] Department of Ophthalmology, Icahn School of Medicine at Mount Sinai Hospital, One Gustave L. Levy Place, Box 1183, New York, NY 10029, USA

ARTICLE INFO

Keywords:
Mathematical model
Blood flow
Oxygenation
Retina
Glaucoma
Flow regulation

ABSTRACT

The retinal vascular network supplies perfusion to vital visual structures, including retinal ganglion cells responsible for vision. Impairments in retinal blood flow and oxygenation are involved in the progression of many ocular diseases, including glaucoma. In this study, an established theoretical hybrid model of a retinal microvascular network is extended to include the effects of local blood flow regulation on oxygenation. A heterogeneous representation of the arterioles based on confocal microscopy images is combined with a compartmental description of the downstream capillaries and venules. A Green's function method is used to simulate oxygen transport in the arterioles, and a Krogh cylinder model is applied to the capillary and venular compartments. Acute blood flow regulation is simulated in response to changes in pressure, shear stress, and metabolism. Model results predict that both increased intraocular pressure and impairment of blood flow regulation can cause decreased tissue oxygenation, indicating that both mechanisms represent factors that could lead to impaired oxygenation characteristic of ocular disease. Results also indicate that the metabolic response mechanism reduces the fraction of poorly oxygenated tissue but that the pressure- and shear stress-dependent response mechanisms may hinder the vascular response to changes in oxygenation. Importantly, the heterogeneity of the vascular network demonstrates that traditionally reported average values of tissue oxygen levels hide significant localized defects in tissue oxygenation that may be involved in disease processes, including glaucoma. Ultimately, the model framework presented in this study will facilitate future comparisons to sectorial-specific clinical data to better assess the role of impaired blood flow regulation in ocular disease.

1. Introduction

Open angle glaucoma (OAG) is one of the most common causes of vision impairment worldwide. Despite its impact, a reliable, non-invasive, and predictive assessment tool for determining individual risk for the onset and progression of OAG has not been realized. The only approved therapy for glaucoma is the reduction of intraocular pressure (IOP); however, many patients either do not exhibit elevated IOP or experience continued disease progression despite medically reduced IOP. Vascular and metabolic abnormalities, including impaired ocular blood flow and retinal oxygenation, have been associated with the onset and progression of OAG for decades [1]. In addition to lower levels of blood flow and metabolism, patients with OAG have also demonstrated impaired vascular regulation in both systemic and ocular tissues [2,3]. While vascular contributions to ophthalmic disease are well established, translating them into a useable format for clinicians has remained elusive. A challenge exists to quantify and understand the contribution of such hemodynamic impairments to retinal function and glaucomatous damage in OAG patients, alone or in combination with IOP and other patient-specific factors. Modeling for clinical impact requires consideration of the dynamic interactions between IOP and ocular hemodynamics and their individual and combined weight on tissue health and resiliency.

Pilot data have indicated an association between vascular biomarkers and OAG, but the large longitudinal population-based data on ocular hemodynamics required to confirm that impaired ocular blood flow and vascular autoregulation are significant primary contributors to OAG disease are currently unavailable. In addition, many shorter duration studies have limited imaging data that are constrained to a single tissue location and/or very brief period of assessment. Traditional observations of the retinal vasculature *in vivo* provide averaged measurements of partial pressure of oxygen (PO_2) in the retinal vasculature,

* Corresponding author.
E-mail address: jarciero@iupui.edu (J. Arciero).
[1] Contributed equally as senior authors.

https://doi.org/10.1016/j.mbs.2023.108969
Received 25 August 2022; Received in revised form 17 January 2023; Accepted 17 January 2023
Available online 23 January 2023

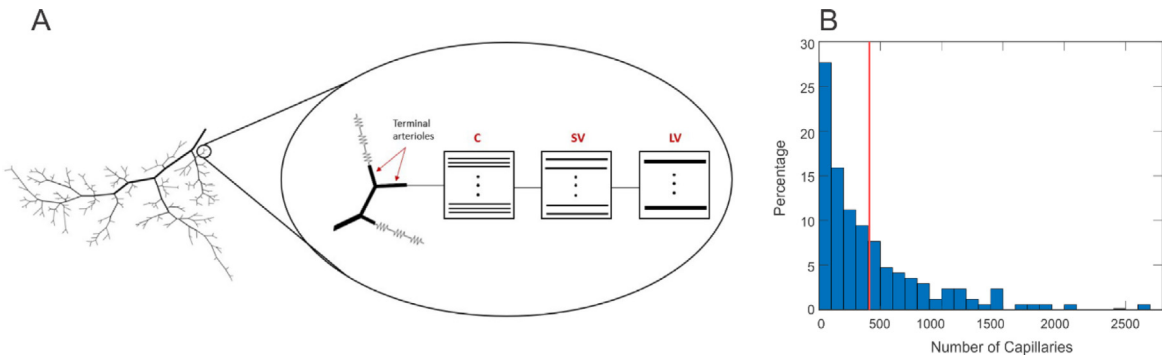

Fig. 1. A. Single branch of the hybrid model [5]. Each terminal arteriole is connected to three compartments representing capillaries (C), small venules (SV), and large venules (LV), as depicted in the inset. B. Histogram representing the number of capillaries (n_C) in each compartment connected to the terminal arterioles. Red line indicates the mean number of capillaries.

but these fail to provide a complete picture of the oxygenation status of ocular tissue, especially since local tissue ischemia has been shown to cause retinal ganglion cell death [1,4]. Mathematical models have emerged as a valuable tool to overcome these challenges and provide a method for predicting and identifying specific localized regions of poor oxygenation that cannot be observed clinically or identified from averaged measurements. We hypothesize that, in diseases such as glaucoma, such regions with reduced oxygenation may relate to loss of vision function despite exhibiting average tissue PO_2 values that are not alarming. By quantifying regions of tissue ischemia and demonstrating the possible mechanisms that lead to the regions of ischemia, mathematical models may provide a clinically relevant method using hemodynamic factors as key predictors of OAG progression. Of note, the inclusion of vascular factors may be of higher significance in persons of African descent who experience significant disease disparities in both glaucoma and systemic vascular disease [1].

Comprehensiveness in a retinal model of hemodynamics is a key aspect to making translational inclusion of vascular outcomes in ophthalmic disease modeling. Various mathematical models of the retina have incorporated some of the key components of the retinal vascular network, including its heterogeneity [6,7], flow regulation [8,9], and oxygen transport [6–8,10]. The current study builds upon our previous work [10,11] to create a theoretical representation of the human retinal vasculature that combines all three of these components. To the best of our knowledge, a model with a heterogeneous vascular structure that accounts for oxygen transport and a mechanistic description of flow regulation does not exist and thus represents a new and relevant tool for understanding the clinical pathophysiology of OAG. Importantly, our mathematical model is based on physical laws and is used to identify a mechanistic explanation for observations of impaired ocular blood flow. The model established in this study will ultimately help to explain why medically lowered IOP does not always prevent the progression of glaucoma, highlight the importance and mechanistic impact of hemodynamic factors in the pathophysiology of glaucoma, and facilitate targeted treatment plans for individual patients.

2. Methods

2.1. Model geometry

The hybrid model geometry employed in this study combines a heterogeneous network structure for arterioles with compartments for capillaries and venules, as shown in Fig. 1A and detailed in [5]. A series of resistors (compartments) representing capillaries, small venules, and large venules is connected downstream of each terminal arteriole (TA) of the heterogeneous arteriolar network. Each resistor (compartment) is comprised of a set of identical, parallel-arranged vessel segments that are assumed to experience the same hemodynamic and metabolic conditions [12,13]. In particular, flow in a single capillary (Q_C) is fixed based on an assumed capillary diameter (6 μm), shear stress (15 dyn/cm^2), and viscosity (9.05 cP), as described in [5]. Thus, by conservation of flow, the number of capillaries in any given compartment is given by $n_{c,i} = Q_{TA,i}/Q_C$, where $Q_{TA,i}$ is flow through the i'th terminal arteriole. Fig. 1B provides a histogram depicting the number of capillaries ($n_{C,i}$) comprising the capillary compartments attached to each of the 171 terminal arterioles, with a mean of 412 capillaries per compartment and a maximum number of 2627 capillaries and minimum number of 9 capillaries.

While the main spatial heterogeneity resides in the arteriolar network, fractional flows (with respective oxygenation levels) enter each set of capillaries downstream of the terminal arterioles. A histogram illustrating the PO_2 levels at the downstream end of the capillaries is provided in Fig. 2 to demonstrate the range of oxygen levels downstream of the site of principal oxygen exchange (i.e., downstream of the capillaries).

For an assumed pressure drop of 16 mmHg along the arteriolar network (i.e., the change in pressure from the end of the central retinal artery to the upstream end of the capillaries, as in [8]), a total flow of 44,805 nL/min is predicted, which is consistent with flows measured in human retina [14–25]. The diameter scaling factor used to transform the mouse vascular network model to the human vascular network model (described in [5]) is increased here from 3.6 to 3.85 to yield this total flow value that is more consistent with reports from recent *in vivo* studies. The resulting arteriolar diameter values remained within the range given in [26] and are provided in Table 1. The original form of this hybrid model [5] includes all four main arterial branches from the central retinal artery. To conserve computation time, a single branch (Fig. 1A) is simulated in this study; total flow along the single branch is predicted to be 14,752 nL/min for a fixed pressure drop of 16 mmHg. Predictions obtained in the single branch are illustrative of outcomes that would be obtained from the entire network.

2.2. Hemodynamics

In the hybrid model, the arteriolar network is represented as a directed graph, where the edges of the graph correspond to the blood vessel segments, each of which has a corresponding diameter and length. Blood flow through each of the vessels is driven by pressure and modeled using Poiseuille's Law: $Q = \Delta P \frac{\pi D^4}{128 \mu L}$, where Q is the blood flow in an individual vessel, ΔP is the pressure drop along the vessel, D is the vessel diameter, L is the vessel length, and μ is the apparent viscosity, which is assumed dependent on the blood vessel diameter and hematocrit based on a previously established empirical relationship from Pries et al. [27].

At every internal node in the network, conservation of mass is assumed, which allows for the flows, pressures, hematocrits, and apparent viscosities to be calculated in each arteriolar segment of the

Table 1
Order, initial (reference) diameter, and number of arterioles in human retinal vascular network.

Order	Branch 1		Branch 2		Branch 3		Branch 4	
	Diameter (μm)	Number	Diameter (μm)	Number	Diameter (μm)	Number	Diameter (μm)	Number
5	117.12	7	103.33	6	92.48	6	109.65	6
4	72.61	10	69.22	9	61.64	9	75.31	4
3	44.43	25	46.89	12	44.16	12	42.54	13
2	30.57	76	30.3	48	30.92	48	30.84	69
1	22.14	220	22.14	136	22.14	102	22.14	147

network, given prescribed pressures at the boundary nodes, using an iterative scheme [28] (described in detail in [10]). At the output of each terminal arteriole, the calculated flow and pressure is used as the input flow and pressure to the corresponding downstream capillary compartment. Then conservation of mass and Poiseuille's Law are again used to compute the flow rates in the downstream compartmental network. Specifying prescribed pressures at the arteriole outflow nodes is needed to couple the two methods for the heterogeneous arteriolar network and the downstream capillary and venular compartments (i.e., the inflow and outflow boundary conditions have to be specified for each of the two methods, and the outflow boundary conditions of the arteriolar network serve as the inflow boundary conditions for the downstream compartments).

2.3. Oxygen transport

The steady-state diffusion of oxygen in the tissue is assumed to be governed by the following equation:

$$D_{diff}\alpha\nabla^2 P_{O_2} = M(P_{O_2}) \tag{1}$$

where P_{O_2} is the partial pressure of oxygen, D_{diff} and α are the diffusivity and solubility of oxygen in the tissue, respectively, and $M(P_{O_2})$ is the tissue oxygen consumption rate. The oxygen consumption rate in the tissue is assumed to have a Michaelis–Menten-type dependence on PO_2, giving

$$M\left(P_{O_2}\right) = M_0 \frac{P_{O_2}}{P_0 + P_{O_2}} \tag{2}$$

where M_0 is the maximum tissue oxygen consumption rate (herein referred to as oxygen demand) and P_0 is the PO_2 at which the consumption rate is half-maximal. Here, it is assumed that $D_{diff}\alpha = 6$ x 10^{-10} cm^3 O_2/cm/s/mmHg [29,30] and $P_0 = 10$ mmHg [31].

To solve Eq. (1) in the spatially heterogeneous arteriolar network, a Green's function method [32,33] is used, where the vessels are represented as discrete oxygen sources, and the tissue points are represented as oxygen sinks [10,11,32,33]. The PO_2 at a given tissue point is then determined as the superposition of the oxygen fields (Green's functions) resulting from the surrounding sources and sinks. This method accounts for the diffusive interactions among all vessels and tissue points throughout the network and is amenable to parallelization, allowing for more efficient computation.

To calculate the source and sink strengths, it is assumed that both the O_2 flux and PO_2 at the blood-tissue interface are continuous. By conservation of mass, in each vessel segment,

$$\frac{df(P_b)}{ds} = -q_v(s) \tag{3}$$

where $f(P_b) = Q(H_D C_0 S(P_b) + \alpha_b P_b)$ is the convective O_2 transport rate, H_D is the discharge hematocrit, C_0 is the hemoglobin-bound O_2 concentration in a fully saturated red blood cell, P_b is the blood PO_2, α_b is the solubility of O_2 in blood, s is the length along the vessel segment, $q_v(s)$ is the rate of diffusive O_2 efflux per unit length, and $S(P_b)$ is the oxyhemoglobin saturation. It is assumed that $S(P_b)$ is a function of blood PO_2 by a Hill equation:

$$S\left(P_b\right) = \frac{P_b^n}{P_b^n + P_{50}^n} \tag{4}$$

where $P_{50} = 26$ mmHg and $n = 2.7$ [34].

Oxygen extraction fraction (OEF) is a parameter defined as the ratio of oxygen consumption to oxygen delivery (as defined in [35,36]). This can be expressed as the ratio

$$OEF = \frac{Blood\,Flow \cdot Arteriovenous\ O_2\ Content\ Difference}{Blood\,Flow \cdot Arterial\ O_2\ Content} \tag{5}$$

In this study, OEF is therefore calculated according to:

$$OEF = \frac{\sum_{i=1}^{n} Q_i \cdot (SaO_2 - SaCV_i)}{Q_{total} SaO_2} \tag{6}$$

where n is the number of terminal arterioles, SaO_2 is the incoming oxygen saturation to the arteriolar network (0.92), $SaCV_i$ is the oxygen saturation at the downstream end of the capillaries along pathway i, and Q_{total} is the total flow into the arteriolar branch.

In the downstream venous and capillary compartments, similarly to Eq. (3), conservation of mass gives the following rate of change of O_2 flux:

$$\frac{d(Q_j H_D C_0 S\left(P_b(s)\right))}{ds} = -q_v(s) \tag{7}$$

where j indicates the index of a given compartment, and s is the length along the compartment.

Oxygen consumption in the capillary compartments is calculated with a Krogh cylinder model [37], whereby each capillary is assumed to deliver oxygen via diffusion to a surrounding tissue cylinder, governed by

$$D_{diff}\alpha\left[\frac{1}{r}\frac{d}{dr}\left(r\frac{dP_{O_2}(s,r)}{dr}\right)\right] = M(P_{O_2}) \tag{8}$$

where r is the radial distance into the tissue cylinder. The oxygen consumption per vessel length is computed according to

$$\int_{r_v}^{r_t} M\left(P_{O_2}\right) 2\pi\, r dr \tag{9}$$

where r_v denotes the radius of the capillary, and r_t denotes the radius of tissue. The width of tissue surrounding each capillary is defined as $d = r_t - r_v$ and is chosen to be 22 μm, as in [5]. Since oxygen is exchanged primarily in the arterioles and capillaries, oxygen exchange in the venular compartments is neglected, and d is set to zero.

2.4. Blood flow regulation

A previous theoretical model of blood flow and oxygen transport in the retinal microcirculation [5,10,11] is adapted here to simulate blood flow regulation in the retinal arterioles. Briefly, wall mechanics within the vessel wall are modeled according to the Law of Laplace, which dictates that the circumferential tension generated within the vessel wall must balance the difference between the pressure inside the vessel and the pressure outside the vessel so that the diameter (D) of the vessel is maintained. The total tension $\left(T_{total} = T_{pass} + AT_{act}^{max}\right)$ that is developed within the vessel wall is modeled as the sum of passive tension (due to structural components and modeled by an exponential function of diameter, $T_{pass} = C_{pass} \exp\left[C'_{pass}\left(\frac{D}{D_0} - 1\right)\right]$) and active tension (due to contraction of smooth muscle cells and modeled by the product of a

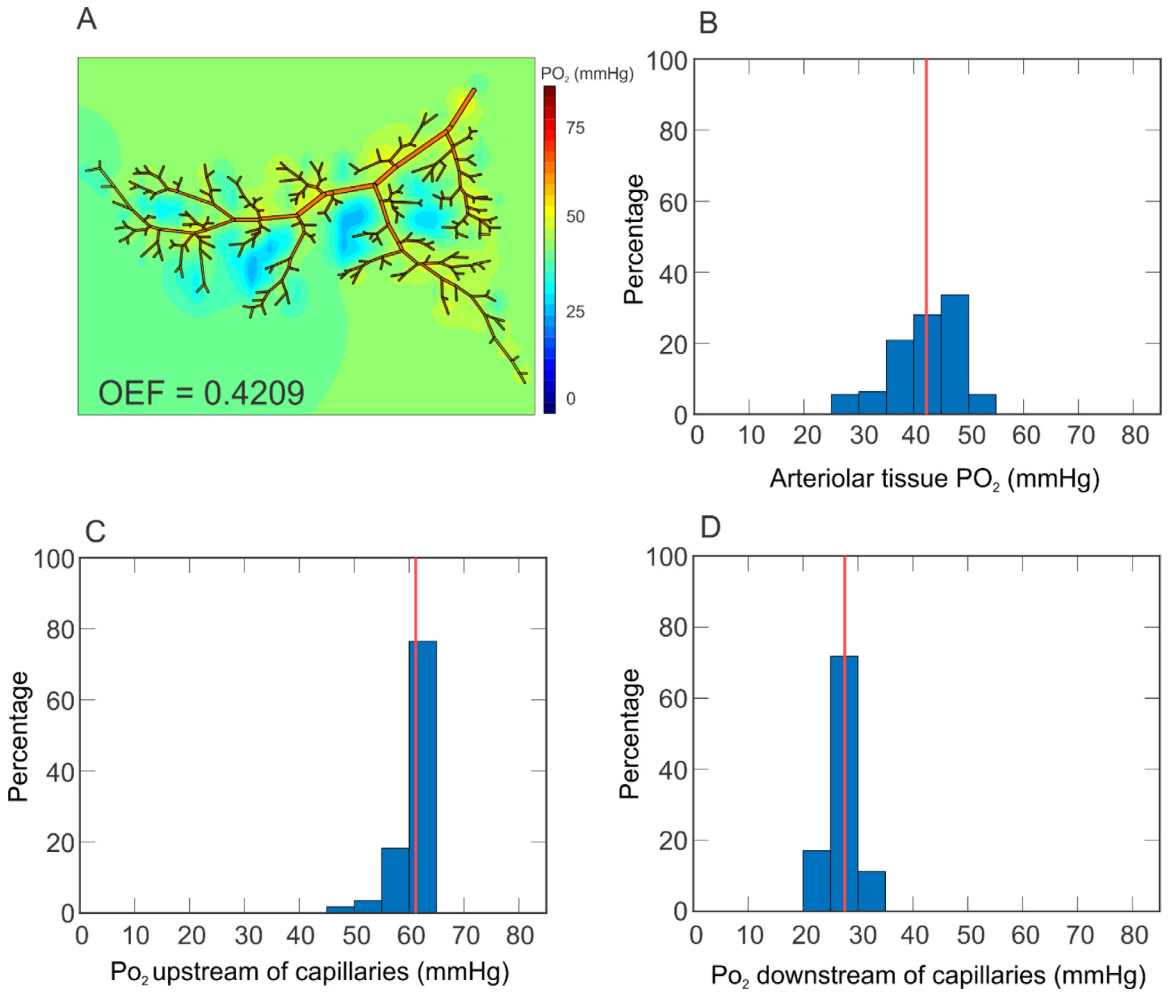

Fig. 2. A. Arteriolar tissue PO_2 levels predicted using the hybrid model for a moderate level of tissue demand ($M_0 = 2$ cm^3 O_2/100 cm^3/min) and IOP = 15 mmHg. A color bar provides the scale for PO_2 levels in mmHg. B. Histogram summarizing the range of arteriolar tissue PO_2 levels predicted by the model in panel A. C. Histogram summarizing the range of vessel PO_2 levels at the upstream end of the capillaries. D. Histogram summarizing the range of vessel PO_2 levels at the downstream end of the capillaries. In all cases, the red line indicates the mean value.

Gaussian function of diameter, $T_{act}^{max} = C_{act} \exp\left[-\left(\frac{\frac{D}{D_0} - C'_{act}}{C''_{act}}\right)^2\right]$, and a sigmoidal function representing the activation, A_{total} (Eq. (10)), of vascular smooth muscle). The myogenic (pressure), shear stress (flow), and conducted metabolic (PO_2) responses combine in an equation for the stimulus for tone (S_{tone}, Eq. (11)) to cause a change in activation and, thus, vessel diameter.

$$A_{total} = \frac{1}{1 + \exp\left(-S_{tone}\left(T_{total}\right)\right)} \tag{10}$$

$$S_{tone} = C_{myo} T_{total}(D) - C_{shear} \tau_{wall}(D, Q) - C_{meta} S_{meta}\left(PO_2\right) + C''_{tone} \tag{11}$$

An increase in activation causes an increase in active tension (vasoconstriction), and a decrease in activation causes a decrease in active tension (vasodilation). The details of this wall mechanics model have been published previously by our group [5,8,11]. Table 2 lists the parameters used in the regulation model.

2.5. Simulations

The incoming arteriolar pressure to the hybrid model is set to 40 mmHg, based on outgoing pressure measurements of the central retinal artery. A pressure drop of 16 mmHg is assumed from the inflow arteriole to the end of the terminal arterioles (i.e., upstream end of the capillaries), consistent with the network from [8]; the venular outlet pressure is set to 15 mmHg so that it is equal to the assumed baseline IOP. The inflow arteriolar blood is assumed to exhibit an oxyhemoglobin saturation of 0.92 (and corresponding blood PO_2 of 64.2 mmHg) [40,41]. The model is simulated under baseline conditions to predict the typical spread of tissue PO_2 throughout the arteriolar network. To determine the effects of IOP and blood flow regulation on retinal tissue oxygenation, the model is then simulated for healthy or elevated levels of IOP (15 and 25 mmHg, respectively) when all regulation mechanisms are present or absent. To further determine the effects of individual regulation mechanisms on blood and tissue oxygenation, M_0 is varied between 1 and 4 cm^3 O_2/100 cm^3/min as in [42], and simulations are run with individual mechanisms turned on and off.

3. Results

The model-predicted tissue and blood oxygenation levels are depicted in Fig. 2 for a moderate level of oxygen demand, $M_0 = 2$ cm^3 O_2/100 cm^3/min. The color map (panel A) shows a range of arteriolar tissue PO_2 levels depending on position. Fig. 2B quantifies this spread using a histogram to indicate the PO_2 level at each arteriolar tissue point modeled in the retina. Although the mean tissue PO_2 level is 42.3 mmHg (with standard deviation of 6.0), the histogram shows a wide spread of predicted values between 26.6 and 51.5 mmHg. Figs. 2C and 2D provide additional histograms for the vessel PO_2 levels at the

Table 2
Parameter values for oxygen transport, conducted metabolic response, and wall tension.

Description	Parameter	Value	Unit	Reference
VSM activation sensitivity	C_{myo}	$1.37/D_0$	cm/dyn	[38]
VSM shear stress sensitivity	C_{shear}	0.0258	cm2/dyn	[8]
VSM metabolic sensitivity	C_{meta}	1000	1/μM/cm	[39]
VSM constant	C''_{tone}	52.2–205.2	–	Calculated
Passive tension strength	C_{pass}	$5.67 \cdot D_0$	dyn/cm	[38]
Passive tension sensitivity	C'_{pass}	$-0.0270 \cdot D_0$	–	[8]
Max active peak tension	C_{act}	$1.30 \cdot D_0^{1.48}$	dyn/cm	[38]
Max active length dependence	C'_{act}	$-0.00146 \cdot D_0 + 1.13$	–	[8]
Max active tension range	C''_{act}	$-0.00146 \cdot D_0 + 0.308$	–	[8]
Passive reference diameter	D_0	30.65–156.02	μm	Calculated

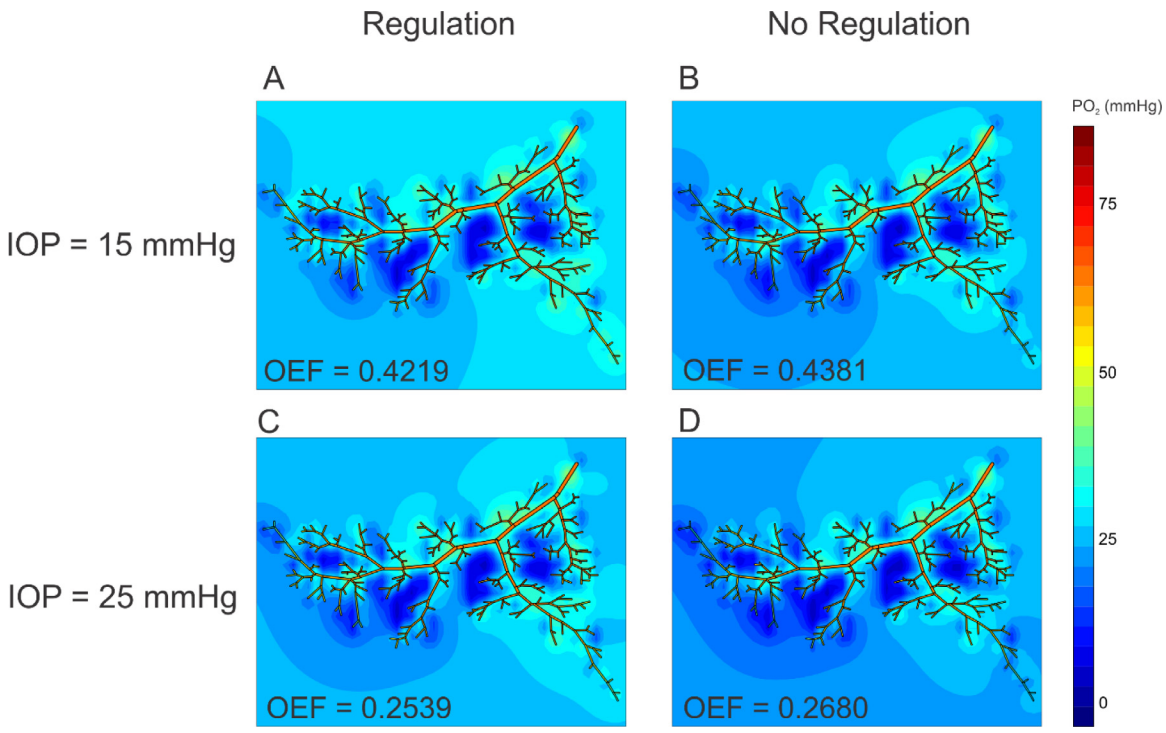

Fig. 3. Arteriolar tissue PO_2 levels predicted using the hybrid model for IOP = 15 mmHg (panels A and B) and IOP = 25 mmHg (panels C and D) in the presence (column 1) or absence (column 2) of blood flow regulation mechanisms with an assumed tissue oxygen demand of $M_0 = 4$ cm^3 O_2/100 cm^3/min. Oxygen extraction fractions (OEF) for each case are also provided.

upstream and downstream ends of the capillaries, respectively. The oxygen extraction fraction (Eq. (6)) for this simulation is provided in panel A.

Fig. 3 shows the model-predicted tissue PO_2 levels in the arteriolar network for different levels of IOP (IOP = 15 mmHg in row 1 and IOP = 25 mmHg in row 2) in the presence (column 1) or absence (column 2) of blood flow regulation mechanisms with an assumed tissue oxygen demand of M_0 = 4 cm^3 O_2/100 cm^3/min. The model predicts a 4% decrease in average tissue oxygenation as IOP is increased from 15 to 25 mmHg. A greater decrease of 6% is predicted in average tissue oxygenation when the flow regulation response mechanisms to pressure, shear stress, and metabolism are inhibited. In addition to changes in average tissue PO_2, increased IOP and inhibited flow regulation also yielded increases in the fraction of arteriolar tissue with low PO_2. In the case with normal IOP (15 mmHg) and regulation present (Fig. 3A), the model predicts the fraction of tissue with a PO_2 less than 20 mmHg to be 20%. When IOP is increased to 25 mmHg (with regulation, Fig. 3C), this fraction increases to 24%. When regulation mechanisms are inhibited (and IOP = 15 mmHg, Fig. 3B), the fraction increases to 25.2%. As expected, this fraction is largest (31.2%) when both IOP is increased to 25 mmHg and regulation is inhibited (Fig. 3D). These changes in tissue PO_2 can be observed in Fig. 3 by the marked increase in sections of the contour map with darker blue color. Oxygen extraction fractions for each simulation are also provided on the contour maps.

To investigate the effects of individual flow regulation mechanisms on the overall regulatory response, simulations were run with and without the various regulatory components of S_{tone} (i.e., the myogenic, shear, and metabolic components). Fig. 4 shows the predicted flow-weighted mean arteriolar diameter as M_0 is increased from 1 to 4 cm^3 O_2/100 cm^3/min, in the cases with no regulation mechanisms present (No regulation, black), all regulation mechanisms present (Myo + Shear + Meta, red), and only the metabolic mechanism present (Meta, blue). As M_0 increases, the inclusion of flow regulation response mechanisms predictably causes an increase in arteriolar diameter. More interesting is that the model predicts a larger increase in arteriolar diameter with only the metabolic mechanism present than with all mechanisms present, indicating that inclusion of the myogenic and shear mechanisms leads to a less robust response than just the metabolic mechanism by itself.

Fig. 5 shows the percentage of arteriolar tissue with a PO_2 less than a given value (PO_2 threshold) for an oxygen demand of M_0 = 2 cm^3 O_2/100 cm^3/min (blue) and $M_0 = 4$ cm^3 O_2/100 cm^3/min (red) and in the presence of only the metabolic response (i.e., no shear or myogenic response, solid) or in the absence of the metabolic response (i.e., only shear and myogenic responses present, dashed). For both levels of

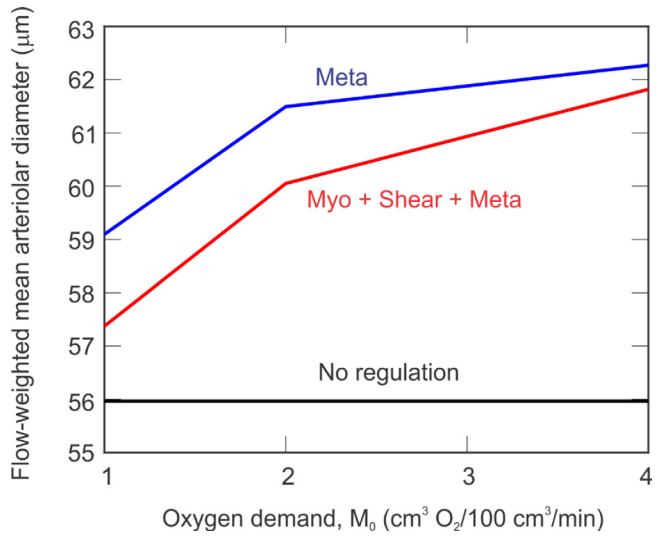

Fig. 4. Flow-weighted mean arteriolar diameter as a function of low, moderate, and high levels of oxygen demand (M_0 = 1, 2, and 4 cm^3 O_2/100 cm^3/min, respectively). The impact of the following flow regulation responses is depicted: metabolic response alone (Meta, blue), no regulation (black), and all regulation responses (Myo + Shear + Meta, red).

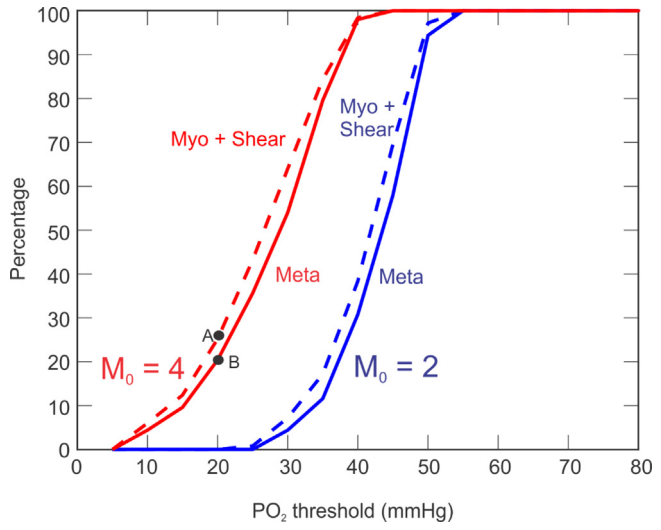

Fig. 5. Percentage of arteriolar tissue exhibiting a PO_2 level at a specific threshold for two levels of oxygen demand (M_0 = 2 (blue) and 4 (red) cm^3 O_2/100 cm^3/min). Curves are shown if only the metabolic response is active (solid) and if only the myogenic and shear responses are active (dashed) to help quantify the utility of the metabolic response.

oxygen demand, there is a higher percentage of tissue with a PO_2 below any given threshold when the metabolic response mechanism is absent (indicated by the dashed curve always lying above the solid curve). As expected, the curves are shifted to the left towards lower PO_2 values with an increase in M_0. Interestingly, the gap between the dashed and solid curves is maintained for a higher M_0, indicating that the metabolic wall mechanism may serve to prevent abnormally low PO_2 levels in the tissue. For example, for M_0 = 4 cm^3 O_2/100 cm^3/min, the model predicts the fraction of arteriolar tissue with PO_2 less than 20 mmHg to be decreased by nearly twenty percent with the inclusion of the metabolic regulation response (see points A and B in Fig. 5).

Fig. 6 further demonstrates the impact of the metabolic response on tissue oxygenation given an oxygen demand of M_0 = 4 cm^3 O_2/100 cm^3/min. As seen in panels A and B, inclusion of the myogenic and shear regulation mechanisms does very little to improve tissue oxygenation. Inclusion of the metabolic regulation mechanism (panel C) both increases the average tissue PO_2 by 6% and decreases the fraction of tissue with PO_2 less than 20 mmHg by 21%. A lower oxygen extraction fraction in the presence of all mechanisms (or metabolic alone) is indicative of the importance of the regulatory capacity of the vasculature.

4. Discussion

Maintaining adequate oxygenation in the retinal vasculature is essential for preserving the health of the eye [1]. This study adapts a previous heterogeneous model of the retinal vasculature [5,10,11] to include blood flow regulation mechanisms in order to explore the combined and/or isolated effects of blood flow regulation, IOP, and oxygen demand on the spatial distribution of oxygenation in a realistic retinal microvascular network.

This study demonstrates the utility of a mathematical model of the retinal microvasculature to identify factors that impact the oxygenation and health of the human retina, including within specific localized regions. For example, this model demonstrates that both increased IOP and impaired flow regulation mechanisms can cause decreased retinal tissue oxygenation (Fig. 3). The model predicts that the absence of flow regulation yields slightly lower tissue oxygenation levels than increased IOP, but both factors are shown to lead to impaired oxygenation characteristic of ocular disease. Importantly, the heterogeneity of the vascular network demonstrates that traditionally reported average values of tissue PO_2 levels hide significant localized defects in tissue oxygenation that may be involved in ocular disease processes, including OAG. Specifically, a lack of flow regulation is predicted to have a greater impact on the fraction of low tissue PO_2 than on the overall average tissue PO_2; thus, only considering average PO_2 changes may be obscuring more significant damage occurring in localized regions/patches. Developing methodology to discriminate localized tissue metabolic disturbances at the site of first tissue loss from global averages may improve translational use of vascular biomarkers in glaucoma by identifying patients at elevated risk for localized vascular insult.

An important use of mathematical models is their ability to isolate and identify key effects of specific factors through multiple simulations. Here, the model was used to assess the contributions of the individual mechanisms involved in the regulation of blood flow throughout the network. Fig. 4 shows that the model predicts a larger increase in diameter in response to increasing oxygen demand when only the metabolic signal is present, compared to when all regulation mechanisms are present. In addition, Fig. 6 shows that the model predicts greater overall oxygenation in the network with only the metabolic regulation mechanism, compared to the case with all mechanisms present. Taken together, these results imply that the myogenic and shear mechanisms may be hindering the regulatory response to increased oxygen demand and decreased oxygenation.

The regulatory effect of the metabolic wall regulation mechanism was further investigated by comparing the fraction of arteriolar tissue with a PO_2 less than a given threshold, in the presence or absence of the metabolic wall mechanism, as oxygen demand was increased (Fig. 5). In addition to an expected decrease in overall oxygenation as oxygen demand was increased (indicated by the leftward shift of the curves), the model consistently predicted a difference between the fraction of tissue less than a given level in the cases with and without the metabolic wall mechanism included. Thus, perhaps more important than causing an increase in average tissue PO_2, the metabolic wall mechanism may serve to prevent tissue hypoxia, as suggested by other recent theoretical modeling results [43]. Given that the metabolic wall signal is conducted upstream in the network to coordinate a response to decreased oxygenation, an impairment to this metabolic signaling (e.g., from endothelial cell dysfunction) could be implicated as a cause of impaired blood flow and oxygenation seen in glaucoma.

Limitations. This hybrid model improves upon previous theoretical models of blood flow regulation in the retina [5,8,10,11] with a full

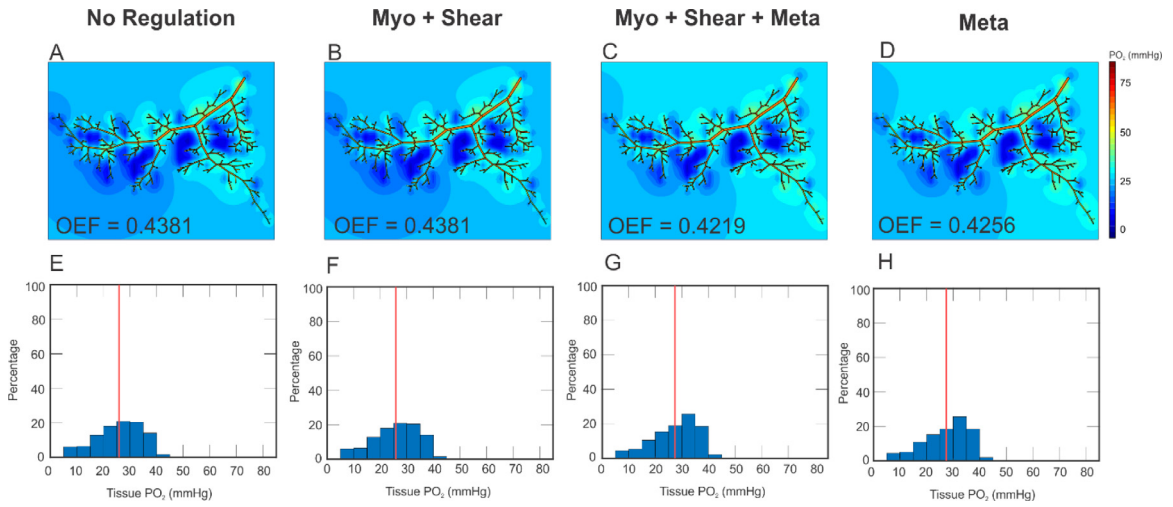

Fig. 6. A–D. Arteriolar tissue PO_2 levels predicted using the hybrid model for varied response mechanisms: no regulation (A), myogenic and shear responses (B), all regulation responses (C), and only the metabolic response (D). Oxygen extraction fractions (OEF) are provided for each case. **E-H.** Histograms depicting the spread of arteriolar tissue PO_2 levels for each case in the top row. Mean arteriolar tissue PO_2 values are depicted with solid red lines. In all cases, oxygen demand is $M_0 = 4$ cm^3 O_2/100 cm^3/min.

description of the microcirculation that includes a heterogeneous arteriolar network; however, a limitation of the model is the lack of heterogeneity in the description of the downstream capillary and venular compartments. Nevertheless, each individual venular compartment associated with each terminal arteriole is different from every other such venular compartment. The current hybrid model description also requires the coupling of oxygen transport methods (Green's function in arterioles and Krogh cylinders in capillaries/venules), causing pressures to be fixed at three levels (inlet of arterioles, outlet of arterioles, and veins). A future model extension will implement a full heterogeneous representation of the downstream venular network and will be used to compare results to the current study. The current model also does not explicitly account for the spatial locations of the downstream capillaries; in particular, capillaries in the superficial, intermediate, and deep layers of the retina may experience different conditions and have different properties which are not considered. Thus, another extension of this model will include a multilayer description of the retinal microcirculation to depict the spatial variation in capillary distribution more accurately.

5. Conclusions

Impairments in retinal blood flow and oxygenation have been implicated in numerous eye diseases, with especially strong data implicating its importance in glaucoma. A comprehensive understanding of hemodynamic factors requires accounting for the dynamic interplay between IOP, blood flow, and tissue metabolism. Here, the first theoretical model to include a heterogeneous vascular network structure, oxygen transport, and blood flow regulation mechanisms is used to demonstrate that retinal tissue oxygenation can be negatively impacted by impairments in blood flow regulation. Importantly, this model not only identifies specific regions of low oxygenation but also predicts the mechanisms causing such reductions. The model has the ability to predict hypoxic regions related to loss of vision function that reside in tissue with average PO_2 values that fall within expected ranges. Finally, the model is used to demonstrate that high IOP is not necessary to yield areas of low PO_2; in fact, the impaired flow regulation leads to larger impairments in tissue oxygenation than elevated IOP, providing possible insight into why lowering medical IOP may not be sufficient in the treatment of all glaucoma cases.

Declaration of competing interest

The authors declare that they have no known competing financial interests or personal relationships that could have appeared to influence the work reported in this paper.

Data availability

Data will be made available on request.

Acknowledgments

AH and BS acknowledge Research to Prevent Blindness.

Funding

JA gratefully acknowledges NSF DMS-1654019 and NSF DMS-1852146. JA, BF, AH, BS, and AV gratefully acknowledge NIH R01EY 030851. AH also acknowledges NSF DMS (1853222/2021192), NYEE Foundation grant, and a Challenge Grant award from Research to Prevent Blindness, NY.

References

[1] A. Harris, et al., Ocular blood flow as a clinical observation: Value, limitations and data analysis, Prog. Retin. Eye Res. (2020) 100841.
[2] S.L. Hosking, et al., Ocular haemodynamic responses to induced hypercapnia and hyperoxia in Glaucoma, Br. J. Ophthalmol. 88 (3) (2004) 406–411.
[3] D. Sines, et al., The response of retrobulbar vasculature to hypercapnia in primary open-angle Glaucoma and ocular hypertension, Ophthalmic Res. 39 (2) (2007) 76–80.
[4] R.N. Weinreb, A. Harris, Ocular Blood Flow in Glaucoma, in: World Glaucoma Association Consensus Series, Kugler Publications, Amsterdam, the Netherlands, 2009.
[5] J. Arciero, B. Fry, A. Albright, G. Mattingly, H. Scanlon, M. Abernathy, B. Siesky, A.V. Vercellin, A. Harris, Metabolic signaling in a theoretical model of the human retinal microcirculation, Photonics 8 (2021) 409.
[6] P. Causin, et al., Blood flow mechanics and oxygen transport and delivery in the retinal microcirculation: Multiscale mathematical modeling and numerical simulation, Biomech. Model Mechanobiol. 15 (3) (2016) 525–542.
[7] D. Liu, et al., Computational analysis of oxygen transport in the retinal arterial network, Curr. Eye Res. 34 (11) (2009) 945–956.
[8] J. Arciero, et al., Theoretical analysis of vascular regulatory mechanisms contributing to retinal blood flow autoregulation, Invest. Ophthalmol. Vis. Sci. 54 (8) (2013) 5584–5593.
[9] G. Guidoboni, et al., Intraocular pressure, blood pressure, and retinal blood flow autoregulation: A mathematical model to clarify their relationship and clinical relevance, Invest. Ophthalmol. Vis. Sci. 55 (7) (2014) 4105–4118.
[10] B.C. Fry, et al., Predicting retinal tissue oxygenation using an image-based theoretical model, Math. Biosci. 305 (2018) 1–9.
[11] B.C. Fry, et al., Blood flow regulation and oxygen transport in a heterogeneous model of the mouse retina, Math. Biosci. 329 (2020) 108476.
[12] J.C. Arciero, B.E. Carlson, T.W. Secomb, Theoretical model of metabolic blood flow regulation: Roles of ATP release by red blood cells and conducted responses, Am. J. Physiol. Heart Circ. Physiol. 295 (4) (2008) H1562–71.

[13] B.E. Carlson, J.C. Arciero, T.W. Secomb, Theoretical model of blood flow autoregulation: Roles of myogenic, shear-dependent, and metabolic responses, Am. J. Physiol. Heart Circ. Physiol. 295 (4) (2008) H1572–9.
[14] J.E. Grunwald, J. DuPont, C.E. Riva, Retinal haemodynamics in patients with early diabetes Mellitus, Br. J. Ophthalmol. 80 (4) (1996) 327–331.
[15] V. Doblhoff-Dier, et al., Measurement of the total retinal blood flow using dual beam Fourier-domain Doppler optical coherence tomography with orthogonal detection planes, Biomed. Opt. Express 5 (2) (2014) 630–642.
[16] C.E. Riva, et al., Blood velocity and volumetric flow rate in human retinal vessels, Invest. Ophthalmol. Vis. Sci. 26 (8) (1985) 1124–1132.
[17] G. Garhofer, et al., Retinal blood flow in healthy young subjects, Invest. Ophthalmol. Vis. Sci. 53 (2) (2012) 698–703.
[18] B. Pemp, et al., Retinal blood flow in type 1 diabetic patients with no or mild diabetic retinopathy during euglycemic clamp, Diabetes Care 33 (9) (2010) 2038–2042.
[19] Y. Wang, et al., Measurement of total blood flow in the normal human retina using Doppler Fourier-domain optical coherence tomography, Br. J. Ophthalmol. 93 (5) (2009) 634–637.
[20] R.M. Werkmeister, et al., Retinal oxygen extraction in humans, Sci. Rep. 5 (2015) 15763.
[21] B. Baumann, et al., Total retinal blood flow measurement with ultrahigh speed swept source/Fourier domain OCT, Biomed. Opt. Express 2 (6) (2011) 1539–1552.
[22] Y. Wang, et al., Pilot study of optical coherence tomography measurement of retinal blood flow in retinal and optic nerve diseases, Invest. Ophthalmol. Vis. Sci. 52 (2) (2011) 840–845.
[23] C. Dai, et al., Absolute retinal blood flow measurement with a dual-beam Doppler optical coherence tomography, Invest. Ophthalmol. Vis. Sci. 54 (13) (2013) 7998–8003.
[24] B. Lee, et al., En face Doppler optical coherence tomography measurement of total retinal blood flow in diabetic retinopathy and diabetic Macular Edema, JAMA Ophthalmol. 135 (3) (2017) 244–251.
[25] S. Srinivas, et al., Measurement of retinal blood flow in normal Chinese-American subjects by Doppler Fourier-domain optical coherence tomography, Invest. Ophthalmol. Vis. Sci. 56 (3) (2015) 1569–1574.
[26] N. Popovic, S. Vujosevic, T. Popovic, Regional patterns in retinal microvascular network geometry in health and disease, Sci. Rep. 9 (1) (2019) 16340.
[27] A.R. Pries, T.W. Secomb, Blood flow in microvascular networks, in: R.F. Tuma, W.N. Duran, K. Ley (Eds.), Handbook of Physiology: Section 2, the Cardiovascular System, IV, Mircrocirculation, Academic Press, San Diego, CA, 2008, pp. 3–36.
[28] D.M. Young, Iterative methods for solving partial difference equations of elliptic type, Trans. Amer. Math. Soc. 76 (1954) 92–111.
[29] M.L. Ellsworth, A.S. Popel, R.N. Pittman, Assessment and impact of heterogeneities of convective oxygen transport parameters in capillaries of striated muscle: Experimental and theoretical, Microvasc. Res. 35 (3) (1988) 341–362.
[30] T.B. Bentley, H. Meng, R.N. Pittman, Temperature dependence of oxygen diffusion and consumption in mammalian striated muscle, Am. J. Physiol. 264 (6 Pt 2) (1993) H1825–30.
[31] A.S. Golub, R.N. Pittman, Oxygen dependence of respiration in rat spinotrapezius muscle in situ, Am. J. Physiol. Heart Circ. Physiol. 303 (1) (2012) H47–56.
[32] R. Hsu, T.W. Secomb, A Green's function method for analysis of oxygen delivery to tissue by microvascular networks, Math. Biosci. 96 (1) (1989) 61–78.
[33] T.W. Secomb, et al., Green's function methods for analysis of oxygen delivery to tissue by microvascular networks, Ann. Biomed. Eng. 32 (11) (2004) 1519–1529.
[34] A.S. Popel, Theory of oxygen transport to tissue, Crit. Rev. Biomed. Eng. 17 (3) (1989) 257–321.
[35] P.Y. Teng, et al., Inner retinal oxygen extraction fraction in rat, Invest. Ophthalmol. Vis. Sci. 54 (1) (2013) 647–651.
[36] K. Pappelis, N.M. Jansonius, Retinal oxygen delivery and extraction in ophthalmologically healthy subjects with different blood pressure status, Transl Vis Sci Technol 11 (2) (2022) 9.
[37] A. Krogh, The number and distribution of capillaries in muscles with calculations of the oxygen pressure head necessary for supplying the tissue, J. Physiol. 52 (6) (1919) 409–415.
[38] B.C. Fry, T.K. Roy, T.W. Secomb, Capillary recruitment in a theoretical model for blood flow regulation in heterogeneous microvessel networks, Physiol. Rep. 1 (3) (2013) e00050.
[39] T.K. Roy, A.R. Pries, T.W. Secomb, Theoretical comparison of wall-derived and erythrocyte-derived mechanisms for metabolic flow regulation in heterogeneous microvascular networks, Am. J. Physiol. Heart Circ. Physiol. 302 (10) (2012) H1945–52.
[40] A. Geirsdottir, et al., Retinal vessel oxygen saturation in healthy individuals, Invest. Ophthalmol. Vis. Sci. 53 (9) (2012) 5433–5442.
[41] F.C. Delori, Noninvasive technique for oximetry of blood in retinal vessels, Appl. Opt. 27 (6) (1988) 1113–1125.
[42] S. Cassani, J.C. Arciero, G. Guidoboni, S. Siesky, A. Harris, Theoretical predictions of metabolic flow regulation in the Retina, Model. Artif. Intell. Ophthalmol. 1 (2) (2016).
[43] B.C. Fry, T.W. Secomb, Distinct roles of red-blood-cell-derived and wall-derived mechanisms in metabolic regulation of blood flow, Microcirculation 28 (5) (2021) e12690.